Disruption of fragmented parent bodies as the origin of asteroid families

Patrick Michel*, Willy Benz† & Derek C. Richardson‡

* *Observatoire de la Côte d'Azur, BP 4229, 06304 Nice cedex 4, France*
† *Physikalisches Institut, University of Bern, Sidlerstrasse 5, CH-3012 Bern, Switzerland*
‡ *Department of Astronomy, University of Maryland, College Park, Maryland 20742-2421, USA*

Asteroid families are groups of small bodies that share certain orbit[1] and spectral properties[2]. More than 20 families have now been identified, each believed to have resulted from the collisional break-up of a large parent body[3] in a regime where gravity controls the outcome of the collision more than the material strength of the rock. The size and velocity distributions of the family members provide important constraints for testing our understanding of the break-up process, but erosion and dynamical diffusion of the orbits over time can erase the original signature of the collision[4,5]. The recently identified young Karin family[6] provides a unique opportunity to study a collisional outcome almost unaffected by orbit evolution. Here we report numerical simulations modelling classes of collisions that reproduce the main characteristics of the Karin family. The sensitivity of the outcome of the collision to the internal structure of the parent body allows us to show that the family must have originated from the break-up of a pre-fragmented parent body, and that all large family members formed by the gravitational reaccumulation of smaller bodies. We argue that most of the identified asteroid families are likely to have had a similar history.

Using a method and numerical codes that have already allowed us to simulate the formation of major asteroid families in different impact energy regimes[7,8], we have performed several simulations of the Karin family formation. In such events, the parent body is first totally shattered by the shock wave produced by a colliding projectile into very small fragments, which are then ejected into space. Subsequently, as a consequence of their gravitational interactions, many of the fragments reaccumulate, forming the large members of the family.

To study how the collisional outcome depends on the internal structure of the parent body, we considered different models of such a body and searched for the one which, once disrupted, best matches the observed properties of the Karin family. In particular, we considered two kinds of parent bodies, both spherical in shape: (1) purely monolithic, and (2) pre-fragmented (pre-shattered or rubble pile). The motivation for modelling the latter kind comes from previous studies of the collisional evolution of the asteroid belt[9], which suggest that before being dispersed in a large-scale collision, large bodies are likely to have suffered smaller shattering impacts that modified their internal structure. Whereas the internal structure of a monolithic parent body is totally homogeneous, that of a pre-fragmented body is characterized by the presence of fractured zones with no tensile strength. As we shall see, the heterogeneities introduced in this way result in significant changes in the size spectrum of the separate bodies (also called fragments) left after the collision, even though the targets in both cases are completely shattered by the impact. Both types of parent bodies were modelled with material properties corresponding to either basalt or dunite, using the Tillotson[10] or ANEOS[11] equations of state, respectively. The corresponding reference bulk densities of these materials are 2.7 g cm^{-3} for basalt and 3.33 g cm^{-3} for dunite, which are within the range of estimated bulk densities of S-type asteroids[12,13] and ordinary chondrites[14].

The diameter of the Karin parent body was inferred from the estimated sizes of the observed members of the family plus a reasonable estimate of the observational incompleteness of the main belt for asteroids with absolute magnitude $H < 16.0$ to account for undetected members. This method gives a parent body diameter D of about 24.5 $\pm$ 1 km, the largest remnant being estimated to account for 47 $\pm$ 6% of its mass[6].

In our simulations (see Table 1), we consider a parent body 25 km in diameter represented by 2×10^5 particles. For each model of internal structure, we consider at most two different impact geometries and adjust the projectile's size to yield a largest remnant with mass in agreement with that inferred from observations. In all cases but one, the impact velocity is fixed at 5 km s^{-1}, which corresponds to the average collisional speed in the asteroid belt[15].

In all our simulations, the fragmentation phase driven by the shock wave of the impact and computed using a three-dimensional smoothed particle hydrodynamics (SPH) code[16], leads to the complete pulverization of the parent body down to the resolution limit, which corresponds to a fragment radius around 0.2 km. The subsequent evolution, including fragment collisions and reaccumulations, is then computed with a sophisticated N-body code[17] until the outcome reaches a nearly steady state (typically a few days of simulated real time). At this point, gravitational reaccumulation has led to the formation of a full size spectrum of aggregates (also called fragments), whose properties we compare with the real Karin cluster. For this, we use two different diagnostics: (1) the cumulative size distribution of the fragments; and (2) their ejection velocities, or equivalently, the dispersion of the family in proper orbital element space. However, any attempt to match the observed proper-

Table 1 **Characteristics of the Karin family formation simulations**

Parent body structure	Equation of state	R_{proj} (km)	V_{proj} (km s^{-1})	θ (°)	Q (erg g^{-1})	M_{lr}/M_{pb}	V_{lr} (m s^{-1})	$\langle V_{ej} \rangle$ (m s^{-1})
Monolithic (basalt)	T	1.35	5	0	1.57×10^8	0.52	5.8	18
Monolithic (dunite)	A	1.22	5	0	1.16×10^8	0.54	0.4	19
Monolithic (dunite)	A	3.10	1	0	7.61×10^7	0.50	0.9	18
Monolithic (basalt)	T	1.65	5	45	2.87×10^8	0.50	8.8	19
Monolithic (dunite)	A	1.57	5	45	2.47×10^8	0.52	5.6	14
Pre-shattered (basalt)	T	1.03	5	0	6.97×10^7	0.47	3.7	14
Pre-shattered (dunite)	A	1.13	5	0	9.21×10^7	0.52	3.6	17
Pre-shattered (basalt)	T	1.21	5	45	1.13×10^8	0.51	4.2	15
Pre-shattered (dunite)	A	1.45	5	45	1.95×10^8	0.46	5.0	18
Rubble pile (basalt)	T	1.50	5	45	2.16×10^8	0.49	5.0	14

Three types of parent bodies were considered, differing in their internal structure: monolithic, pre-shattered or rubble pile. To model a pre-shattered parent body, we generated a network of cracks in an originally monolithic body, dividing it into 40 distinct fragments distributed uniformly in radius and separated by fractured zones. Fragment masses were randomly distributed in a range with the maximum mass four times larger than the minimum mass. Experiments with other position and mass distributions produced similar results. To model a rubble pile, we generated solid boulders whose centres were chosen at random inside the parent body, with their individual radii computed from a power-law distribution. In most cases two simulations were performed for each type of parent body, one using material properties of basalt and the Tillotson equation of state (T) and one using dunite and the ANEOS equation of state (A). Different impact conditions were also used, defined by the projectile's radius R_{proj}, impact velocity V_{proj} and angle of incidence θ. The specific impact energy is given by Q = (projectile kinetic energy)/(target mass). M_{lr}/M_{pb} is the resulting mass ratio of the largest remnant to the parent body and V_{lr} is the largest remnant ejection speed. The mean ejection speed of all the fragments is given by $\langle V_{ej} \rangle$.

ties exactly is pointless given the uncertainties in the observational data (for example, sizes are only estimated using inferred albedos), as well as the large number of unknowns characterizing the impact (actual impact velocity, shapes, and so on). That is why we focus more on global characteristics that we believe to be robust, such as the continuous aspect of the cumulative size distribution and the shape of the cluster in proper element space.

In the case of the break-up of monolithic parent body, we find that the cumulative size distribution of fragments is always characterized by a lack of intermediate-sized bodies and a very steep slope for the smaller ones. This trend also holds true for a collision occurring at a smaller (and much less likely) impact speed of $1\,\mathrm{km\,s^{-1}}$ but with a bigger projectile to yield a largest remnant of similar mass (see Fig. 1a, b). Yet the inferred size distribution of the real Karin family is rather continuous (the second-largest body is estimated to have a diameter $D \approx 14.4$ km).

Disruptions involving a pre-fragmented (pre-shattered or rubble pile) parent body, on the other hand, result in a much more continuous cumulative size distribution of fragments (Fig. 1c, d). Hence the presence of intermediate-sized bodies, as observed in the real family, is most probably a direct consequence of the presence of large-scale fractures or big blocks within the parent body. Such large members cannot be obtained starting with a monolithic parent body regardless of the impact geometry and material type in all the cases investigated (not all are shown here), so we conclude that the parent body of the Karin family must have been pre-fractured or reaccumulated. This is consistent with the fact that the Karin parent body actually belonged to the older Koronis family, for which we have shown in previous simulations that the members down to at least kilometre sizes are reaccumulated objects[7,8,16].

Interestingly, we note that intermediate-size fragments are also present in most major asteroid families, which implies that many parent bodies in the asteroid belt were probably pre-fragmented. Consequently, this must also be the case for most large objects in the present-day asteroid belt, which is consistent with the idea that asteroids get battered over time in the general sense.

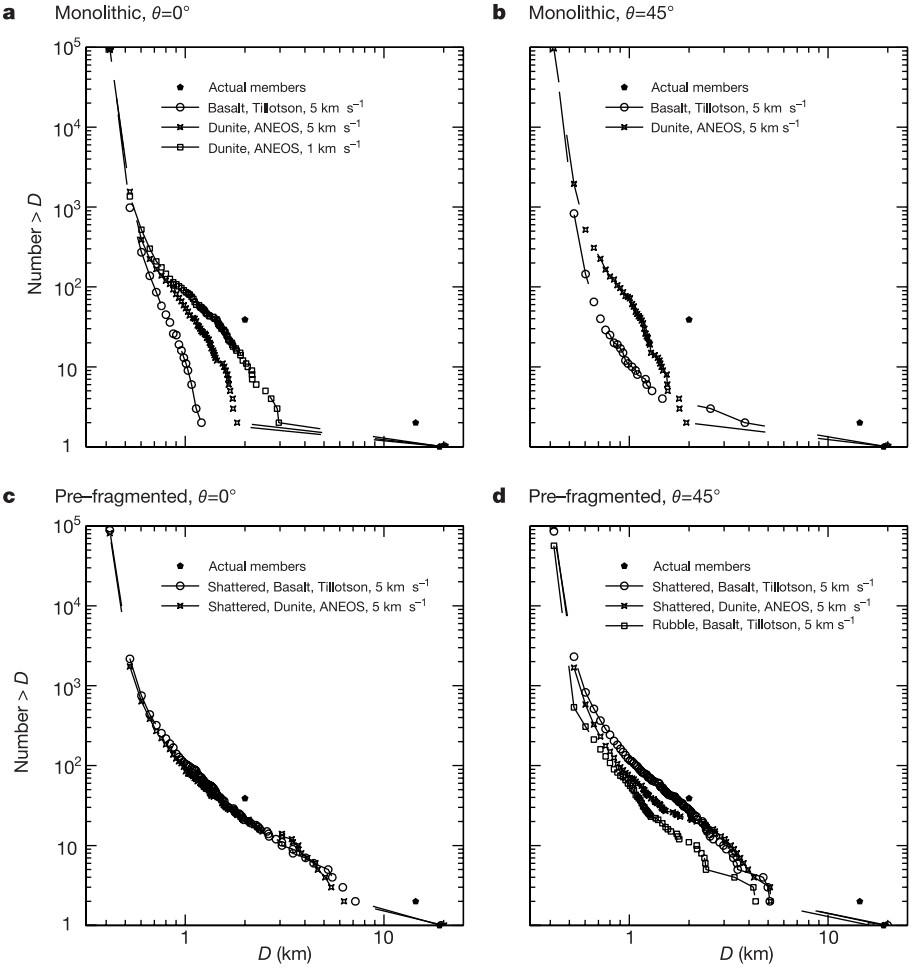

Figure 1 Cumulative diameter distributions of the fragments of the simulated Karin families. **a**, **b**, The disruption of a monolithic parent body; **c**, **d**, the results for a pre-fragmented parent body. **a** and **c** were obtained with a projectile colliding 'head on', whereas an impact with an angle of incidence θ equal to 45° produced **b** and **d**. Symbols denote the different material properties or impact parameters used in the simulations, as indicted on the plots. In all simulations, the parent body had a diameter D equal to 25 km. The plots also show the estimated sizes of the two largest members as well as the number of members larger than 2.1 km (computed from their absolute magnitudes and assuming a 16% albedo for all family members; see ref. 6). The best agreement is obtained with our simulations of the disruption of a pre-fragmented parent body and does not depend much on the impact geometry or the material type and equation of state. Conversely, in the case of a monolithic target, different impact geometries and/or material types and equations of state do not produce more intermediate-sized aggregates, even though some quantitative differences exist. For instance, a 45° impact results in a somewhat smaller gap between the sizes of the largest and the second-largest remnant in the simulation of a basaltic parent body with a Tillotson equation of state. We note that only the simulations involving a pre-fragmented parent body yield continuous size distributions.

The second important constraint we considered was the ejection velocity distribution of simulated fragments, which must be compatible with that of the real family members. Karin's young age (around 5 Myr) implies that dynamical diffusion has had no time to alter appreciably the initial ejection velocity distribution, which is not the case for the other, much older, families. Unfortunately, only the proper orbital elements (semi-major axis a, eccentricity e, and inclination I) of the family members can be deduced from observations, whereas the simulations only provide the ejection velocities. However, Gauss' equations can be used to relate ejection velocities to orbital elements, provided the position of the barycentre of the family in a heliocentric reference frame is known. To solve these equations, two additional unknown angles must be specified, namely the true anomaly f and the argument of perihelion ω of the parent body's orbit at the time of the impact. The current observed shape of the cluster in orbital element space suggests $f = 30°$ and $f + \omega = 45°$ as a good choice[6].

As can be seen from Fig. 2, the dispersion in ejection velocities of fragments originating from a monolithic parent body impacted at 5 km s^{-1} is too small to explain the actual observed spread in proper element space. Conversely, supporting our previous conclusion based on the size distribution, the ejection velocity field obtained in a collision involving pre-fragmented parent bodies is in excellent agreement with the observed family. Such agreement is also obtained from the break-up of a monolithic parent body at low impact speed (1 km s^{-1}); however, as remarked before, in this case the fragment size distribution is not continuous. In summary, a good match of both a continuous size distribution and the orbital

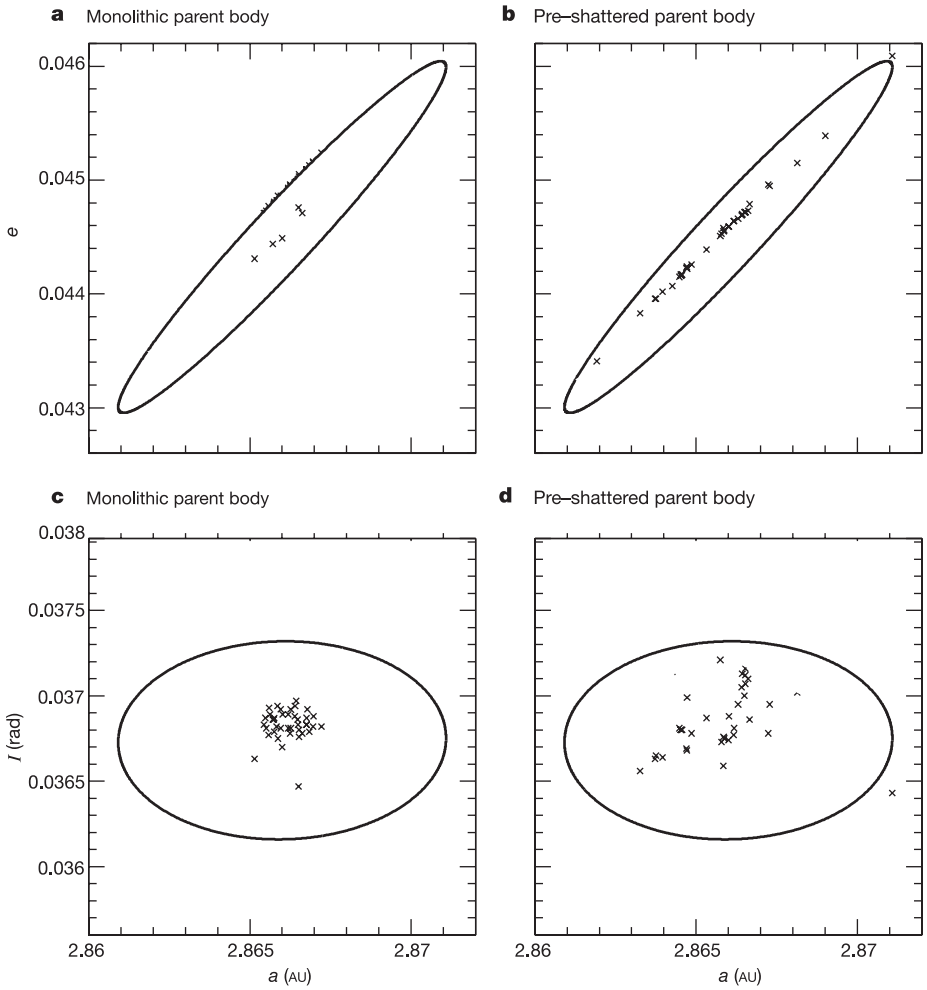

Figure 2 Dispersion of the simulated Karin family in orbital element space. The plots show the distributions in the eccentricity versus semi-major axis plane (**a**, **b**) and in the inclination versus semi-major axis plane (**c**, **d**) obtained by considering either a monolithic parent body (**a**, **c**) or a pre-shattered one (**b**, **d**) of 25 km diameter suffering a 'head-on' collision with a projectile. The ANEOS equation of state was used with material properties of dunite. Because the proper elements of the real family members are not available, and because we are not interested in fitting exactly the position of each real member but rather in reproducing the global dispersion of the Karin family, we show the ellipse already identified[6] as best matching the dispersion of the real family in this space. The orbital elements of fragments are computed from their ejection velocities using Gauss' equations. To convert ejection velocities from our simulations into orbital elements, we first need to define the orientation of the velocity components of our fragments in a heliocentric frame. For this, the reference frame used in our simulations being arbitrary, we must specify the direction of impact of the projectile. Different directions lead to different shapes of the family in orbital element space, so we investigated a range of possible orientations which are then obtained by assuming the values of the semi-major axis and inclination of the projectile's orbit, and using the so-called Tisserand constant as a constraint to fix the eccentricity (see ref. 8 for a description of this procedure). We consider here one possible orientation. Other combinations of the projectile's orbital elements or impact direction would not necessarily lead to the same shape of cluster. The values of the parent body's true anomaly at impact f and its sum with the argument of perihelion $\omega + f$ are assumed to be $f = 30°$ and $\omega + f = 45°$; its semi-major axis a, eccentricity e, and inclination I are taken to be $a = 2.866$ AU, $e = 0.0445$ and $I = 2.105°$. Only 39 real Karin family members are currently known, so the figure also shows the distributions of only the 39 largest fragments of our simulation, the smallest among them having a size of 1.5 km, to be compared to the estimated 2.1 km for the real one. For the projectile, the velocity of impact is 5 km s^{-1}, $\theta = 0°$, $a = 2.2$ AU, and $I = 5°$.

dispersion of the Karin family requires that its parent body was pre-fragmented or reaccumulated. This supports the overall picture that all large members of asteroid families are reaccumulated bodies, given that the Karin cluster is at least a second-generation family in the lineage of the older Koronis parent body.

Our simulations can also be used to determine the impact energy needed to produce a given degree of disruption as a function of the internal structure of the parent body. From Table 1, we see that disrupting a pre-shattered target requires less energy per unit mass than for a monolithic body. This, at first glance a surprising result, is related to the fact that the fractures as modelled here (no porosity and no material discontinuities except damage) do not affect shock waves but only tensile waves. Hence, fragments can be set in motion immediately upon being hit by the shock wave without having to wait for fracture to occur in a following tensile wave. Thus, transfer of momentum is more efficient and disruption facilitated. Note that the presence of large voids such as those in rubble piles affect the propagation of the shock wave, thus reversing this trend. A more detailed study of these properties will be presented in another paper. Nevertheless, it is already clear that the internal structure of an asteroid plays an important role in the determination of its response to impacts (see also ref. 18). This is not only relevant for estimating the collisional lifetime of a body in the asteroid belt, but also for developing strategies to deflect a potential Earth impactor.

A last important implication of our simulations concerns the properties of family members with sizes smaller than can currently be observed. The break-up of a pre-shattered Karin parent body produces several thousand fragments with sizes ranging from a few kilometres down to our resolution limit of 0.2 km (Fig. 1). Their ejection speeds can allow some of them to be injected into efficient transport mechanisms leading to Earth-crossing orbits. Therefore, we conclude that the Karin break-up event may well have produced some near-Earth asteroids and even some meteorities. According to our simulations, the potential near-Earth asteroids with size at least above 0.2 km result from the gravitational reaccumulation of smaller fragments, and are therefore all aggregates. □

Received 4 October; accepted 5 December 2002; doi:10.1038/nature01364.

1. Milani, A. & Knežević, Z. Asteroid proper elements and the dynamical structure of the asteroid main belt. *Icarus* **107,** 219–254 (1994).
2. Zappalà, V., Bendjoya, P., Cellino, A., Farinella, P. & Froeschlé, C. Asteroid families: Search of a 12,487-asteroid sample using two different clustering techniques. *Icarus* **116,** 291–314 (1995).
3. Farinella, P., Davis, D. R. & Marzari, F. in *Completing the Inventory of the Solar System* (eds Rettig, T. W. & Hahn, J. M.) 45–55 (ASP Conference Series 107, Astronomical Society of the Pacific, San Francisco, 1996).
4. Marzari, F., Farinella, P. & Davis, D. R. Origin, aging, and death of asteroid families. *Icarus* **142,** 63–77 (1999).
5. Bottke, W. F., Vokrouhlický, D., Brož, M., Nesvorný, D. & Morbidelli, A. Dynamical spreading of asteroid families via the Yarkovsky effect. *Science* **294,** 1693–1696 (2001).
6. Nesvorný, D., Bottke, W. F., Dones, L. & Levison, H. F. The recent breakup of an asteroid in the main-belt region. *Nature* **417,** 720–722 (2002).
7. Michel, P., Benz, W., Tanga, P. & Richardson, D. C. Collisions and gravitational reaccumulation: Forming asteroid families and satellites. *Science* **294,** 1696–1700 (2001).
8. Michel, P., Benz, W., Tanga, P. & Richardson, D. C. Formation of asteroid families by catastrophic disruption: Simulations with fragmentation and gravitational reaccumulation. *Icarus* **160,** 10–23 (2002).
9. Melosh, J. G. & Ryan, E. V. Asteroids: shattered but not dispersed. *Icarus* **129,** 562–564 (1997).
10. Tillotson, J. H. *Metallic Equations of State for Hypervelocity Impact* (General Atomic Report GA-3216, San Diego, 1962).
11. Thompson, S. L. & Lauson, H. F. Improvement in the chart D radiation hydrodynamic code III: revised analytic equation of state. (Report SC-RR-71 0714, Sandia National Laboratory, Albuquerque, 1972).
12. Belton, B. *et al.* The bulk density of asteroid 243 Ida from Dactyl's orbit. *Nature* **374,** 785–788 (1995).
13. Yeomans, D. K. *et al.* Radio science results during the NEAR-Shoemaker spacecraft rendezvous with Eros. *Science* **289,** 2085–2088 (2000).
14. Flynn, G. J., Moore, L. B. & Klöck, W. Density and porosity of stone meteorites: implications for the density, porosity, cratering, and collisional disruption of asteroids. *Icarus* **142,** 97–105 (1999).
15. Bottke, W. F., Nolan, M. C., Greenberg, R. & Kolvoord, R. A. Velocity distributions among colliding asteroids. *Icarus* **107,** 255–268 (1994).
16. Benz, W. & Asphaug, E. Catastrophic disruptions revisited. *Icarus* **142,** 5–20 (1999).
17. Richardson, D. C., Quinn, T., Stadel, J. & Lake, G. Direct large-scale *N*-body simulations of planetesimal dynamics. *Icarus* **143,** 45–59 (2000).
18. Asphaug, E. *et al.* Disruption of kilometre-sized asteroids by energetic collisions. *Nature* **393,** 437–440 (1998).

Acknowledgements P.M. acknowledges financial support from the Action Thématique Innovante 2001 of the French INSU, the programme 'Bonus-Qualité-Recherches 2001' and the Cassini laboratory of the Côte d'Azur Observatory (OCA). W.B. and D.C.R. acknowledge support respectively from the Swiss National Science Foundation and NASA through the Office of Space Science. Simulations were carried out on 4-processor Compaq DEC Alpha workstations thanks to the SIVAM project and the ILGA team of the OCA and on a Beowulf installed by the society Alineos.

Competing interests statement The authors declare that they have no competing financial interests.

Correspondence and requests for materials should be addressed to P.M. (e-mail: michel@obs-nice.fr).

Attosecond control of electronic processes by intense light fields

A. Baltuška*, Th. Udem†, M. Uiberacker*, M. Hentschel*, E. Goulielmakis*, Ch. Gohle†, R. Holzwarth†, V. S. Yakovlev*, A. Scrinzi*, T. W. Hänsch† & F. Krausz*

** Institut für Photonik, Technische Universität Wien, Gusshausstrasse. 27, A-1040 Wien, Austria*
† Max-Planck-Institut für Quantenoptik, Hans-Kopfermann-Strasse 1, D-85748 Garching, Germany

The amplitude and frequency of laser light can be routinely measured and controlled on a femtosecond (10^{-15} s) timescale[1]. However, in pulses comprising just a few wave cycles, the amplitude envelope and carrier frequency are not sufficient to characterize and control laser radiation, because evolution of the light field is also influenced by a shift of the carrier wave with respect to the pulse peak[2]. This so-called carrier-envelope phase has been predicted[3–9] and observed[10] to affect strong-field phenomena, but random shot-to-shot shifts have prevented the reproducible guiding of atomic processes using the electric field of light. Here we report the generation of intense, few-cycle laser pulses with a stable carrier envelope phase that permit the triggering and steering of microscopic motion with an ultimate precision limited only by quantum mechanical uncertainty. Using these reproducible light waveforms, we create light-induced atomic currents in ionized matter; the motion of the electronic wave packets can be controlled on timescales shorter than 250 attoseconds (250×10^{-18} s). This enables us to control the attosecond temporal structure of coherent soft X-ray emission produced by the atomic currents—these X-ray photons provide a sensitive and intuitive tool for determining the carrier-envelope phase.

Matter exposed to intense laser light undergoes ionization, which gives rise to a broad range of phenomena in atoms, molecules and plasmas. An electronic wave packet is set free around each oscillation peak of a laser electric field that is strong enough to overcome the effective binding potential (Fig. 1a). The ensuing motion of the wave packets released by optical-field ionization depends on the subsequent evolution of the driving laser field[11,12]. A laser pulse consisting of many wave cycles launches a number of wave packets at different instants. Each of these follows a different trajectory because of the differences in the initial conditions of their motion, preventing a precise control of strong-field-induced electronic dynamics. Intense few-cycle light pulses with adjustable carrier-envelope (C-E) phase hold promise for a marked improvement. With the C-E phase set to make the peak of the oscillating electric field coincide with the pulse peak (blue line in Fig. 1c) and the strength of the field just sufficient to reach the ionization threshold